Available online at www.sciencedirect.com
ScienceDirect
Journal of the European Ceramic Society 32 (2012) 157–165
www.elsevier.com/locate/jeurceramsoc

Electrical resistivity of silicon nitride–silicon carbide based ternary composites

Eveline Zschippang [a,*], Hagen Klemm [a], Mathias Herrmann [a], Kerstin Sempf [a], Ulrich Guth [b], Alexander Michaelis [a]

[a] *Fraunhofer Institute for Ceramic Technologies and Systems IKTS, Winterbergstrasse 28, 01277 Dresden, Germany*
[b] *Kurt-Schwabe-Institute for Measuring and Sensor Technology Meinsberg, Ziegra-Knobelsdorf, Germany*

Received 24 February 2011; received in revised form 25 July 2011; accepted 2 August 2011
Available online 30 August 2011

Abstract

New electrically conductive ternary composites were developed by adding 8 vol.% of ZrN or ZrB_2 to a Si_3N_4–SiC matrix. During hot pressing, ZrB_2 reacted with Si_3N_4 to form $ZrSi_2$, ZrN, Si and BN whereas added ZrN did not undergo any reactions in the Si_3N_4–SiC–ZrN composite. The composites modified by ZrN or ZrB_2 addition showed a lower resistivity (7×10^3 Ω cm and 3×10^{-1} Ω cm) compared to the matrix (3×10^4 Ω cm). Further studies on the grain size distribution and the volume ratio of conducting and non-conducting phases excluded a percolation network of ZrN and $ZrSi_2$ grains. In fact, doping of SiC grains and modified grain boundaries as a consequence of the formation of liquid phases during sintering are suggested to be the reason for the significantly lower resistivity of materials containing $ZrSi_2$.

A decrease in the composite resistivity due to a subsequent heat treatment was obtained for all hot-pressed composites.

Keywords: Composite; Si_3N_4; SiC; Electrical resistivity; Microstructure

1. Introduction

Silicon nitride (Si_3N_4) exhibits various outstanding mechanical properties even at high temperatures[1–3] and is therefore used for engine or aerospace components, actually with regard to corrosive and high-temperature environment. Si_3N_4 is an insulator, but by adding a conductive phase into the insulating Si_3N_4 matrix, electrically conductive composites can be formed. The electrical resistivity of a composite is connected to the formation of a percolating network of the electrically conducting phase within the Si_3N_4 matrix and can be described phenomenologically with the percolation theory. The value of the critical volume V_{cr} where a three-dimensional conducting network is formed varies between 1 vol.% and 60 vol.% and strongly depends on the microstructural properties of the composite. In the case of conducting spheres, placed at random in a matrix of insulating spheres of an equal size, and in the case when all neighbouring grains are electrically connected it was found that V_{cr} is 16 ± 2 vol.%.[4,5] Usually, higher values of V_{cr} are obtained attributed to some nearest neighbour grains which fail to connect with each other. Lower values of V_{cr} are reported for composites with high particle size ratios of insulating matrix R_p to conducting particle R_m,[6,7] composites with segregated distribution of conductive particles[7,8] or conducting particles with elongated geometry.[9–11]

A promising candidate for a electrically conductive phase within a Si_3N_4 matrix is silicon carbide (SiC). SiC exhibits similar mechanical properties even at high temperatures and the combination of Si_3N_4 and SiC results in Si_3N_4–SiC composite materials with an electrical resistivity between 10^7 and 10^3 Ω cm.[12,13] Owing to the good high-temperature properties as well as to the electrical properties, composites based on Si_3N_4 and SiC are recommended as heating elements.

However, several applications require composites with a lower electrical resistivity than obtained by Si_3N_4–SiC composites. Si_3N_4 composite materials containing a metal-like conducting phase, such as $MoSi_2$,[14–17] TiN[18–21] or TiB_2,[22] might be an option. These composites possess an electrical resistivity of approximately 10^{-3} Ω cm, but volume fractions of about 30% of the metal-like conducting phase have to be added to

* Corresponding author. Tel.: +49 0351 25 53 7647; fax: +49 0351 25 54 157.
E-mail address: eveline.zschippang@ikts.fraunhofer.de (E. Zschippang).

0955-2219/$ – see front matter © 2011 Elsevier Ltd. All rights reserved.
doi:10.1016/j.jeurceramsoc.2011.08.002

Table 1
Compositions of the composite materials.

Composite	Non-conducting phases (vol.%)		Conducting phases (vol.%)			
	SiO_2/Yb_2O_3	Si_3N_4	SiC	ZrB_2	ZrN	$ZrSi_2$
SC47	9	44	47			
ZB4	9	44	43	4		
ZB8	9	44	39	8		
ZB8-SN	9	83	0	8		
ZB12	9	44	35	12		
ZB20	9	44	27	20		
ZS8	9	44	39			8
ZN8	9	44	39		8	
ZN12	9	44	35		12	
ZN20	9	44	27		20	

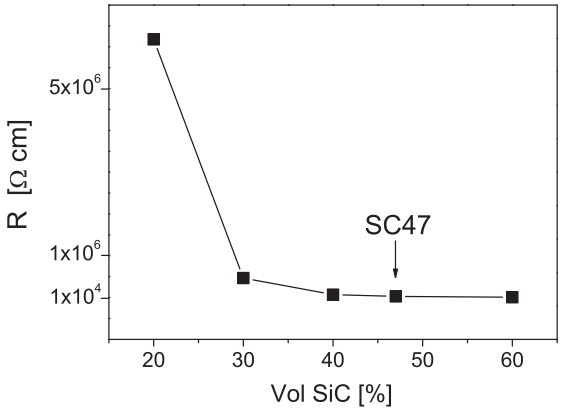

Fig. 1. Room-temperature electrical resistivities of the Si_3N_4–SiC composite inclusive the basic composite SC47.

the matrix. The massive dispersion of the metal-like conducting phase causes alterations of the properties of Si_3N_4 ceramics.[23] Especially, a large CTE (coefficient of thermal expansion) mismatch between Si_3N_4 ($\sim 2.5 \times 10^{-6}\,K^{-1}$)[24] and the conducting fillers ($MoSi_2$: $\sim 8.4 \times 10^{-6}\,K^{-1}$, TiN: $\sim 9.3 \times 10^{-6}\,K^{-1}$)[24] might result in matrix cracking during thermal cycling.[25] Indeed, the amount of metal-like conducting particles can be minimized by reducing the particle size of the metal-like conducting particles, but otherwise the preparation of nanostructured composites implies complexity and costs. The inclusion of a low amount of metal-like conducting particles into a Si_3N_4–SiC composite forming a ternary composite Si_3N_4–SiC–ZrX_z might be an option. The aim of this paper is to evaluate the ternary composites Si_3N_4–SiC–ZrB_2 and Si_3N_4–SiC–ZrN in terms of differences in the electrical resistivity and the percolation behavior of the ZrX_z phases (X = B, N, Si).

2. Experimental

The experiments were started from a basic composite composition of 44 vol.% Si_3N_4 and 47 vol.% SiC (Table 1) with a SiC volume fraction in excess of the percolation threshold (Fig. 1). Additionally, 9 vol.% sintering aids (Yb_2O_3, SiO_2) were added, whereas Yb_2O_3 was chosen as one example of the rare-earth oxides.

4, 8, 12 and 20 vol.% of SiC were replaced by the metal-like conducting phases ZrX_z, i.e. ZrB_2 ($6 \times 10^{-6}\,\Omega\,cm$)[24] or ZrN ($21 \times 10^{-6}\,\Omega\,cm$),[24] in order to obtain composites with nearly the same volume fraction of conducting material (Table 1). Additionally, the composites ZB8–SN (8 vol.% ZrB_2, 0 vol.% SiC) and ZS8 (8 vol.% $ZrSi_2$, 39 vol.% SiC) were investigated to determine the influence of SiC, and in the case of ZS8 the influence of the ZrB_2 decomposition process on the conduction mechanism within the ZB8 composite. The composites were made from commercial Si_3N_4 (Silzot HQ), SiC (HCST, α-SiC, Grade UF 15) and ZrN (ABCR, Grade A) or ZrB_2 (ESK, Typ C) powders. SiO_2 (Heraeus, Pyro Syn) and Yb_2O_3 (Treibach) were added as sintering additives. The starting powders were mixed in isopropanol for 4 h by attrition milling. The slurries were dried in a rotary evaporator and the powder passed through a 400 μm sieve. In addition, the sieved powder was heated up to 800 °C in argon atmosphere to remove the residual organics. All powders were hot pressed in a circular BN-coated graphite tool with a diameter of 80 mm. All composites were sintered at 25 MPa in nitrogen atmosphere at temperatures up to 1840 °C. Specimens of the Si_3N_4–SiC–ZrB_2, Si_3N_4–ZrB_2 and Si_3N_4–SiC–$ZrSi_2$ composites were cut out of the middle of the hot-pressed disc due to an increased formation of ZrN at the rim of the hot-pressed disc (Section 3.1).

One quarter of the hot-pressed discs was heat treated in a gas pressure furnace with a nitrogen pressure of 5 MPa in order to generate a coarser microstructure.

The phase composition of the sintered materials was determined by XRD (CuKα). A quantitative analysis of the phase composition was carried out using the Rietveld method (Autoquan software). Thermodynamic calculations were performed with FactSage 6.1 using the fact database.

The cross sections of the specimens were polished by ion beam technique[26–30] and analyzed using a FESEM. Inlens and SE images were recorded simultaneously and both images were used to distinguish the Si_3N_4, SiC and ZrX_z grains by image processing. The equivalent diameter of the ZrX_z and SiC grains and the thickness of the elongated needle-like Si_3N_4 grains[31] were determined using Leica Software. The electrical resistivity was measured by four-probe method on specimens with a dimension of 4 mm × 4 mm × 20 mm between 20 °C and 800 °C in Ar atmosphere. A silver braze (CB11, Unicore-BrazeTec) was applied as electrical contact. Two contacts were placed at the 4 mm × 4 mm faces and two small dots on one of the 4 mm × 20 mm face. Gold wires were then mounted using an Ag/Pd paste. While the samples were heated in a tube furnace under argon atmosphere, the electrical resistivity and temperature were measured with a multimeter.

3. Results and discussion

3.1. Hot pressing and phase composition

The phase compositions of the hot-pressed composite materials were characterized by X-ray diffraction (Table 2). All hot-pressed composites showed the presence of Si_3N_4, SiC and at least one crystallized intergranular ytterbium-oxide phase

Table 2
Volume fractions of the different phases in the composites after hot pressing and subsequent heat treatment at 1900 °C (HT) determined by XRD quantitative phase analysis.

Composite	Resistivity (Ω cm)	Non-conducting phases (vol.%)			Conducting phases (vol.%)		
		Intergranular phase	Si_3N_4	BN	SiC	Si	ZrN + $ZrSi_2$
SC47	3×10^4	$6Yb_2SiO_5$	45		49		
SC47 HT	4×10^3	$13Yb_4Si_2N_2O_7$	42		45		
ZB4	1×10^1	$4Yb_2SiO_5 + 2$YbSZ	42	3	44	1	1 + 3
ZB8	3×10^{-1}	$5Yb_2SiO_5 + 2$YbSZ	34	9	41	1	2 + 6
ZB8 HT	2×10^{-2}	$1Yb_2SiO_5 + 5Yb_4Si_2N_2O_7 + 2$YbSZ	35	8	39	2	3 + 5
ZB8-SN	$>10^{10}$	$6Yb_2SiO_5$	71	14		2	3 + 4
ZB12	3×10^{-2}	$5Yb_2SiO_5 + 3$YbSZ	34	10	35		2 + 11
ZB20	2×10^{-3}	$6Yb_2SiO_5 + 2$YbSZ	17	28	25		4 + 18
ZS8	4×10^{-1}	$4Yb_2SiO_5 + 1Yb_2Si_2O_7 + 2$YbSZ	45		42		1 + 5
ZS8-HT	3×10^{-2}	$10Yb_4Si_2N_2O_7 + 1$YbSZ	47		37		1 + 4
ZN8	6×10^3	$7Yb_2SiO_5 + 1$YbSZ	46		39		7 + 0
ZN8 HT	2×10^2	$7Yb_4Si_2N_2O_7 + 11Yb_{4.67}(SiO_4)_3O + 1$YbSZ	39		36		6 + 0
ZN12	1×10^3	$6Yb_2SiO_5 + 2$YbSZ	47		35		10 + 0
ZN20	5×10^1	$5Yb_2SiO_5 + 1Yb_2Si_2O_7 + 4$YbSZ	48		24		18 + 0

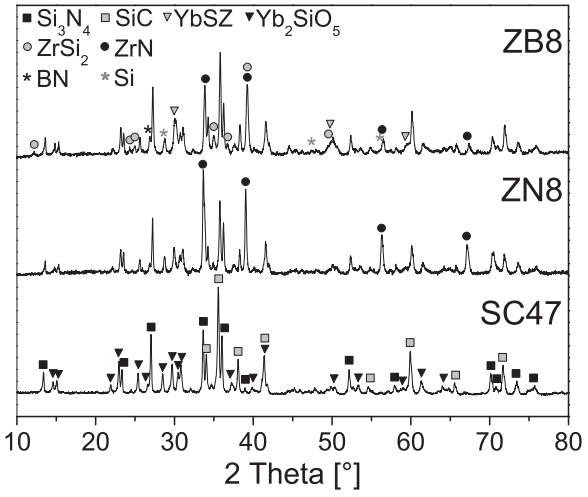

Fig. 2. Phase compositions of SC47, ZN8, ZB8.

(Fig. 2). Additionally, small amounts of ytterbia-stabilized zirconia (YbSZ) were detected. ZrN was found in ZN8, ZN12 and ZN20 whereas no crystalline ZrB_2 phase was found in ZB8, ZB12, ZB20 indicating that ZrB_2 was not stable in the Si_3N_4-SiC composite system. Instead of ZrB_2 crystalline ZrN, $ZrSi_2$ and BN were identified. Additionally, free silicon with a concentration in the range between 1 and 2 vol.% was determined by Rietveld analysis and confirmed by SEM investigations of the microstructure. It can be stated that the Si reflexes adjoin other components reflexes making a precise determination of the Si content more difficult.

The Rietveld analysis indicates that ZrB_2 reacted with Si_3N_4 which is in good agreement with earlier references describing the use of Si_3N_4 as a sintering aid for the densification of transition metal borides (TiB_2, ZrB_2 and HfB_2).[32–37] Thermodynamic calculations of the system Si_3N_4/SiC/ZrB_2 were carried out in the temperature range between 1500 °C and 1840 °C to simulate the reactions taking place during sintering. The overall pressure was set at 1 atm. The oxide and oxonitride phases were not taken into account due to the lack of data. These phases will not influence the reaction of ZrB_2 with Si_3N_4 significantly. The data of ZrC_4 existing in the database were excluded, because they were determined only at low temperatures (below 550 °C) and extrapolation to high temperatures probably results in larger deviations. The calculations with this phase resulted in a high stability of this phase which was not observed experimentally.

The thermodynamic calculations were carried out under different conditions:

(a) with excess of nitrogen and
(b) without an excess of nitrogen.

If an excess of nitrogen exists the equilibrium phases were Si_3N_4, SiC, ZrN and BN in addition to the gas phase.

This can be summarized by the reaction:

$$2ZrB_2 + 3\,N_2 \rightarrow\ 2ZrN\ +\ 4BN \quad (1)$$

Without an excess of nitrogen the decomposition follows another route:

At temperatures below 1660 to 1670 °C ZrB_2 is in equilibrium with Si_3N_4 and SiC. Only above this temperature ZrN, BN and a metallic liquid containing mostly Si, some Zr and B is formed.

$$4ZrB_2 + 3Si_3N_4 \rightarrow\ 4ZrN\ +\ 8BN\ +\ 9Si\,(\text{metallic melt}) \quad (2)$$

Therefore, the formation of the microstructure can be explained as follows:

During the densification in the hot press ZrB_2 only partially reacts with the nitrogen atmosphere according to reaction (1) due to kinetic reasons. In the moment when only closed porosity exists the reaction with nitrogen from atmosphere is nearly stopped due to the much slower diffusion of the nitrogen through the oxonitride liquid in comparison to the gas phase. This is the reason why the material behaves similar to the case without excess of nitrogen, and why a metallic melt containing Si, Zr and partially B is formed in addition to ZrN and BN. The

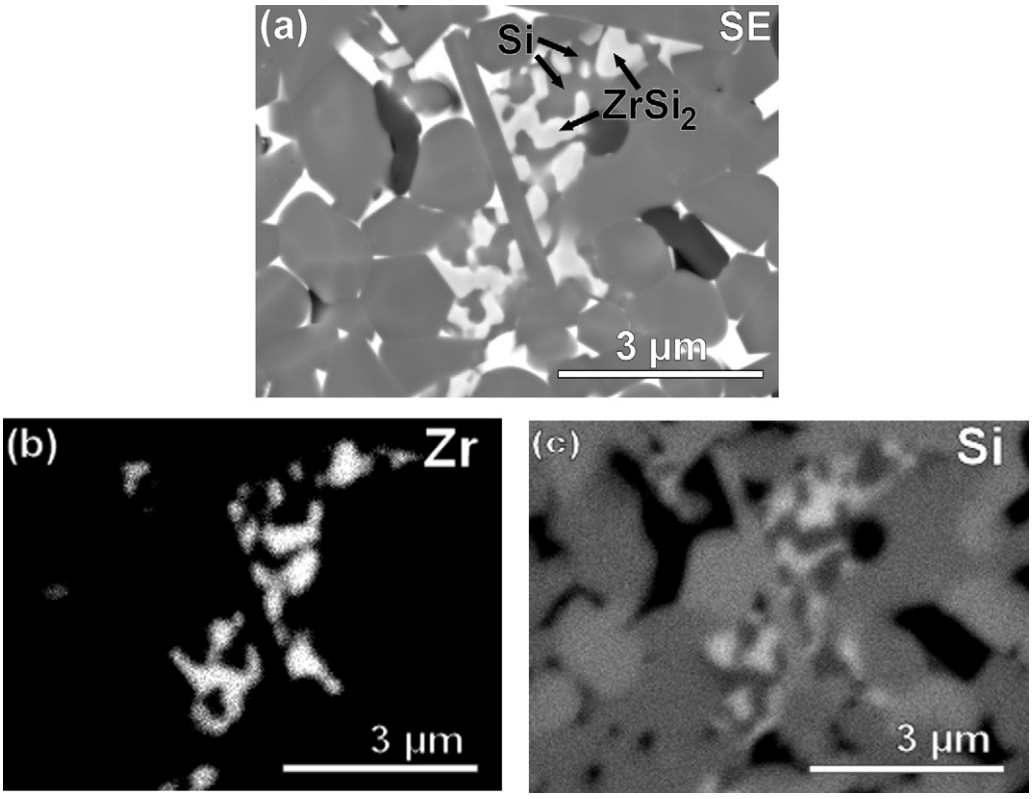

Fig. 3. FESEM and EDX images of ZB8 HT.

liquid Si is additionally stabilized as the activity of the liquid Si is reduced due to the formation of a solution with Zr. The ratio of Si/Zr/B in the melt cannot be predicted by the thermodynamic calculations carried out, because there is no complete and adequate description of the Zr–Si–B melt in the database. From the experimental data it is very likely that the composition of the melt is between Si and $ZrSi_2$, but near to $ZrSi_2$. During cooling this melt cannot react fast enough with the ZrN and BN to form the equilibrium phases at lower temperatures.

In comparison, in terms of a nitrogen pressure of one or even more atmospheres, Si could not be formed due to the fast reaction:

$$Si + N_2 \rightarrow Si_3N_4 \quad (3)$$

It can be determined that this reaction has not happened during the subsequent heat treatment at 1900 °C and 50 atm nitrogen pressure due to the slow diffusion of nitrogen through the sample. Only in the outer rim of the hot-pressed plate a change in the composition according to the thermodynamics was observed. This area was removed and not investigated in detail.

A nitrogen pressure of one atmosphere also leads to the decomposition of $ZrSi_2$ into Si_3N_4 and ZrN. This is in agreement with the fact that $ZrSi_2$ will partially decompose into Si_3N_4 and ZrN (Table 2) during hot pressing of $ZrSi_2$-containing composites.

In spite of the decomposition processes no significant changes in the volume ratios of conducting to insulating phases was obtained (Table 2). The consumption of insulating Si_3N_4 was compensated by the formation of insulating BN. Also the amount of the metal-like conducting phases ZrB_2 (starting powder) and ZrN, $ZrSi_2$ (reaction product) was nearly the same. Because of no remarkable changes in the volume fractions differences in the resistivities between the Si_3N_4–SiC–ZrN and Si_3N_4–SiC–ZrB_2 composites could not be referred to volume changes caused by the decomposition process.

3.2. Electrical properties and percolation behavior

The percolation behavior of a binary Si_3N_4–SiC composite is shown in Fig. 1. By adding a large quantity of SiC the electrical resistivity of the Si_3N_4–SiC composites still remained in the range of $10^4\ \Omega$ cm. To investigate the influence of ZrX_z addition on the Si_3N_4–SiC composite resistivity, 8 vol.% of a metal-like conducting ZrB_2 or ZrN phase was added wherein the Si_3N_4–SiC composite had a SiC fraction in excess of the percolation threshold. By adding the same volume fractions of metal-like conducting phases, the electrical resistivity of the ternary ZN8 and ZB8 composites was $7 \times 10^3\ \Omega$ cm and $3 \times 10^{-1}\ \Omega$ cm, respectively. The values differ nearly in the order of four magnitudes even though ZrN and $ZrSi_2$ inhibit similar electrical resistivities of $2 \times 10^{-5}\ \Omega$ cm[24] and $16 \times 10^{-5}\ \Omega$ cm[24]. The resistivity as a function of temperature is presented in Fig. 4 for the ternary composites and the Si_3N_4–SiC (SC 47) composite. The composites SC47 and ZN8 had a similar resistivity that decreased nonlinearly with increasing temperature. In contrast, the resistivity of ZB8 was less temperature-dependent in the investigated temperature range. To identify the reasons for the different resistivities a detailed study

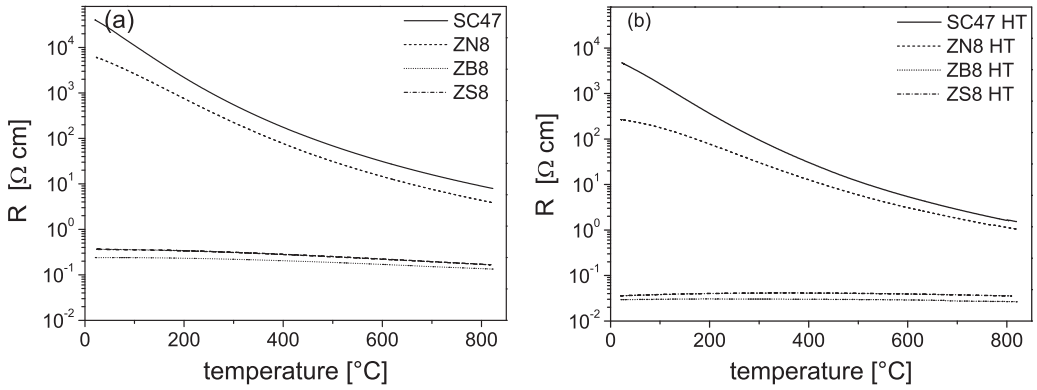

Fig. 4. Electrical resistivities against temperature for SC47, ZN8, ZB8 and ZS8 (a) after hot pressing and (b) after a subsequent heat treatment at 1900 °C.

concerning the percolation behavior of the Si_3N_4–SiC–ZrX_z composites was made by partially exchanging SiC by different amounts of ZrN or ZrB_2. In each case, the volume fraction of electrically conducting phase, SiC plus ZrX_z was kept constant at 47 vol.%. The addition of only small portions of ZrB_2 (ZB4, ZB8) induced a sharp decrease of resistivity from 10^4 Ω cm to 10^{-1} Ω cm (Fig. 5) whereas further addition of ZrB_2 only caused a comparatively slight decrease in the electrical resistivity from 10^{-1} Ω cm (ZB8) to 10^{-3} Ω cm (ZB20). However, it took up to 20 vol.% of ZrN to obtain a resistivity of about 10^{-1} Ω cm which was commensurate with the resistivity of ZB8. A sharp decrease in the resistivity of the ZN composites was observed between ZN12 and ZN20 indicating that there might be a percolation threshold in this range.

An electrical resistivity of about 10^{-1} Ω cm obtained for ZB8 leads to the question if percolation of the ZrX_z grains in the ZB composites might start at volume fractions far from 16 vol.%, a value predicted by percolation theory. If the critical volume (V_{cr}) for ZrX_z percolation in the ZB composites is considerably lower than in the ZN composites, microstructural differences should be distinguishable.

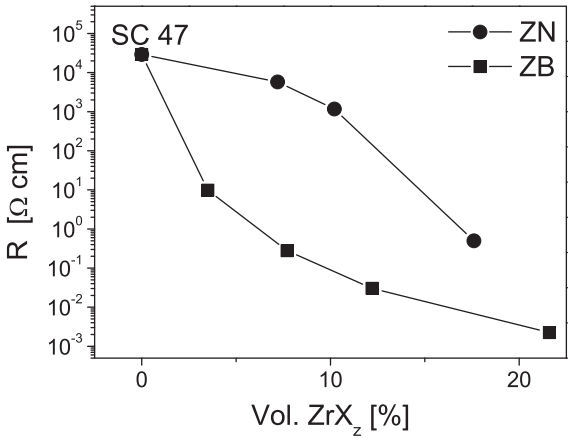

Fig. 5. Room-temperature electrical resistivities of the Si_3N_4–SiC–ZrN and Si_3N_4–SiC–ZrB_2 composites as a function of the adjusted ZrX_z-volume.

3.3. Electrical properties and microstructure

It is well-known that the microstructure and especially the grain size ratio of the insulating matrix to the conducting particle R_p/R_m[6,7] plays a significant role concerning the percolation behavior. To study the influence of the grain size ratio on the composite resistivity, the equivalent diameter of SiC and ZrX_z grains and the thickness of the Si_3N_4 (elongated needle-like[31]) grains were determined. Additionally, the effect of grain growth and the associated changes in the grain size ratios of the hot-pressed composites were investigated by annealing the composites in a gas pressure furnace at 1900 °C in nitrogen atmosphere.

The microstructures of the hot pressed composites and the composites after subsequent heat treatment are shown in Fig. 6a–g.

Using the Inlens mode, the conducting SiC and the highly conducting ZrX_z grains appeared as grey and bright phases. The non-conducting Si_3N_4 grains and the intergranular phases were dark grey. Boron nitride developed during hot pressing in ZB8 appeared as dark platelet-like grains, too.

Some differences were observed in the shape of the ZrX_z grains: the ZrN grains in ZN8 (Fig. 7a) appeared more separated because the contact areas were concave. In contrast, $ZrSi_2$ in ZB8 (Fig. 7b) showed a good wetability on the SiC and some of the SiC grains were even enclosed by $ZrSi_2$. This correlates with the fact that a liquid Zr–Si melt was formed during hot pressing (Section 3.1). Additionally, Figs. 3 and 6e reveal the presence of $ZrSi_2$–Si precipitations. Due to the subsequent heat treatment process at 1900 °C the $ZrSi_2$ grains and these precipitations became liquid again leading to more and larger precipitation structures within the composite (Fig. 6f).

With regard to the different grain size distributions, a cumulative frequency analysis of the ZrX_z and SiC (equivalent) grain diameters and the thickness of the Si_3N_4 grains were performed (Fig. 8) using at least 500 grains in each case. It can be determined that there were smaller ZrX_z grains in ZB8 (median: 0.3 μm) as in ZN8 (median: 0.6 μm) by insignificant differences in the Si_3N_4 thickness (0.4 μm in ZB8 and 0.3 μm in ZN8) and in the SiC diameter (0.4 μm in ZB8 and 0.3 μm in ZN8) leading to a ratio $R_{Si_3N_4}/R_{ZrX_z}$ of about 1 for ZB8 and 2 for ZN8. Due to the subsequent heat treatment, the differences in the ZrX_z grain sizes further increased (0.2 μm in ZB8-HT and 1.5 μm in ZN8-HT) whereas the median value of the SiC

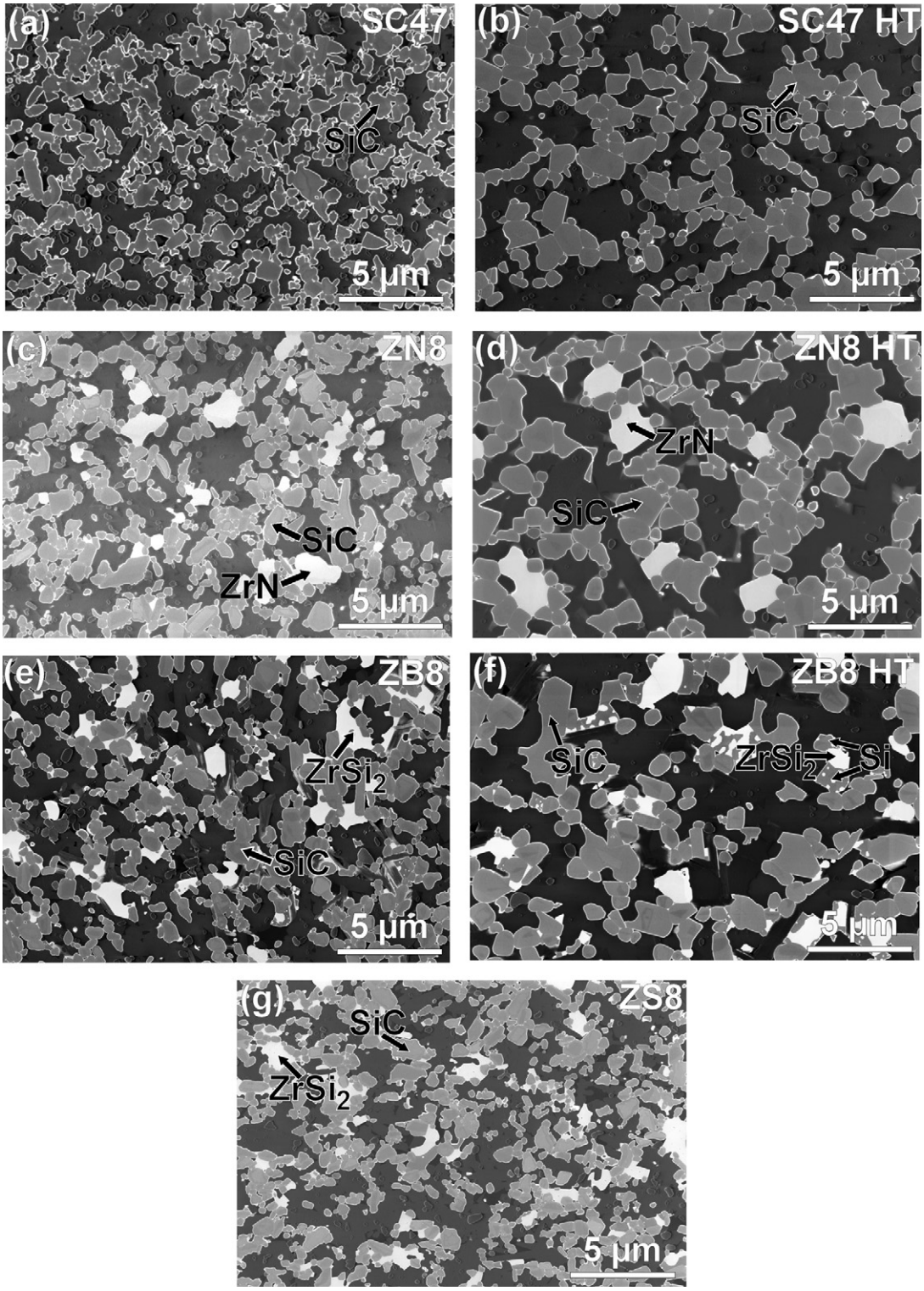

Fig. 6. FESEM Images (Inlens mode) of the composites after hot pressing SC47 (a), ZN8 (c), ZB8 (e), and ZS8 (g), and after a subsequent heat treatment at 1900 °C SC47 HT (b), ZN8 HT (d) and ZB8 HT (f).

grains (0.8 μm in ZB8-HT and ZN8-HT) and the Si_3N_4 thickness (0.8 μm ZB8-HT and 0.7 μm in ZN8-HT) was twice as high in ZB8-HT as well as in ZN8-HT. In spite of the difference in the $R_{Si_3N_4}/R_{ZrX_z}$ ratio, which was 4 for ZB8-HT and 0.5 for ZN8-HT, the resistivity of all heat treated composites was about one order of magnitude smaller (Fig. 4b). This is in accordance with the general trend of polycrystalline SiC showing a decrease in the resistivity due to a subsequent heat treatment.[38,39] On the other hand, the huge difference in the grain size distribution and the median grain size values of ZrX_z in ZB8 and ZN8 might have an influence on the composite resistivity in terms of percolation theory.

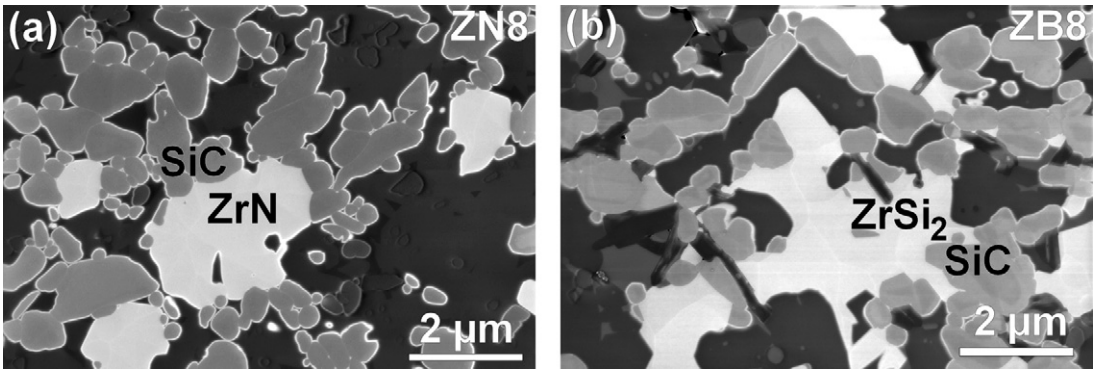

Fig. 7. FESEM Images (Inlens mode) of ZN8 (a) and ZB8 (b).

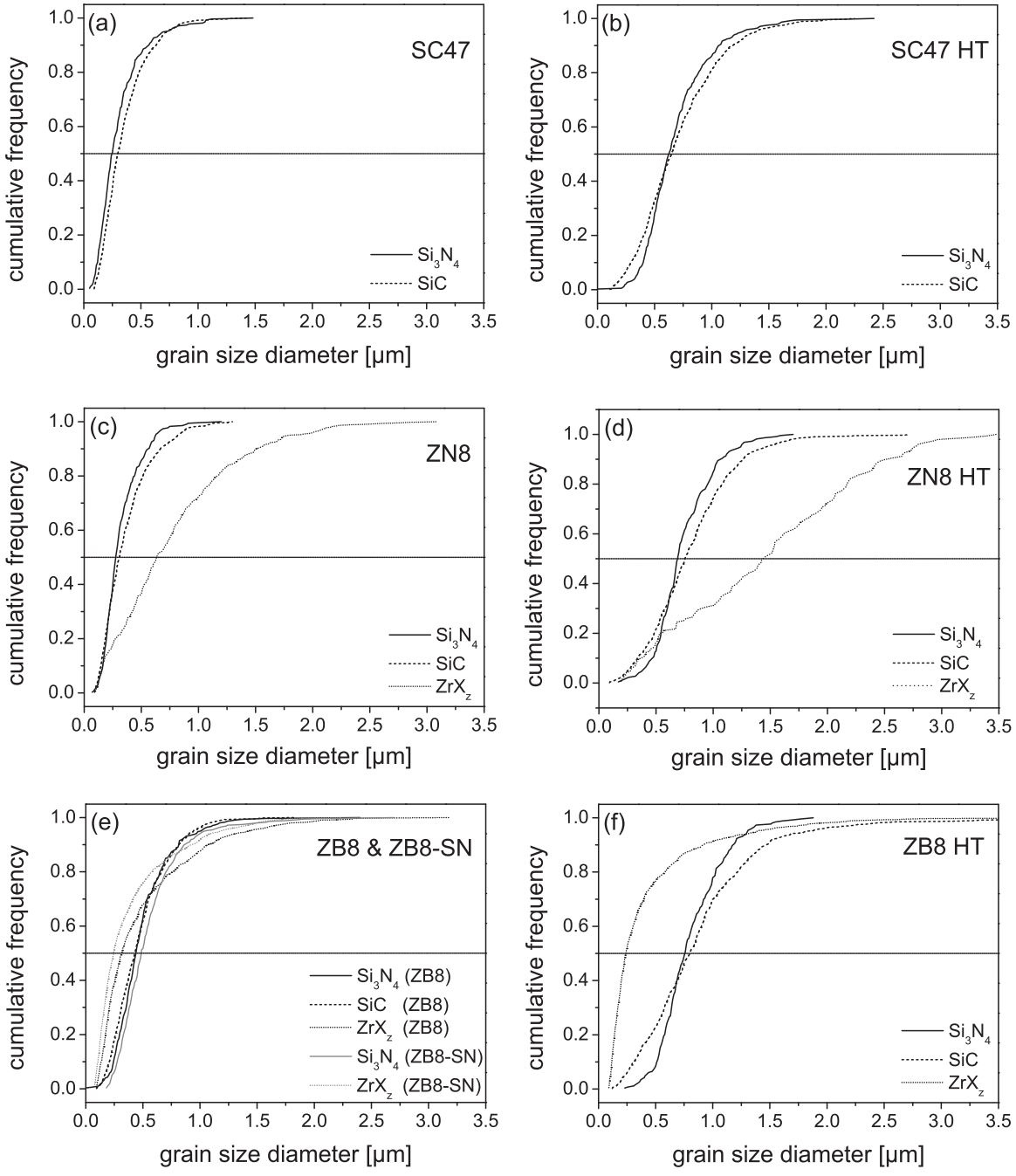

Fig. 8. Cumulative frequency of the ZrX_z, SiC and Si_3N_4 grains in SC47 (a), SC47 HT (b), ZN8 (c), ZN8 HT (d) ZB8 and ZB8-SN (e), and ZB8 HT (f).

To determine the impact of the ZrX_z grains on the conduction mechanism with regard to a ZrX_z percolation, a sample containing 8 vol.% ZrB_2 but no SiC (ZB8-SN) was prepared. Among Si_3N_4 and Yb_2SiO_5 the crystalline phases BN, ZrN, Si and $ZrSi_2$ (Table 2) were found, indicating that the decomposition process was similar to that of the Si_3N_4–SiC–ZrB_2 composites. Furthermore, the grain size distributions of the Si_3N_4 and ZrX_z grains in ZB8 and ZB8–SN (Fig. 8e) did not show significant differences but the electrical resistivity of ZB8–SN was higher than $10^{10}\,\Omega$ cm. Hence, no ZrX_z percolation network was formed in ZB8 suggesting that also no percolation of the ZrX_z grains occurred in ZB8, and that the conducting pathways in ZB8 had to be mainly provided by the SiC grains and ZrX_z grains in addition. An uncertainty in respect of the different $ZrSi_2$:ZrN ratio and a lower amount of $ZrSi_2$ in ZB8–SN compared to ZB8 (Table 2) could not be used to explain the large difference in resistivity since the composite ZB4 containing only 3 vol.% $ZrSi_2$ and 1 vol.% ZrN still revealed a low resistivity of $10^1\,\Omega$ cm. More likely, the differences in the resistivity can be referred to two facts.

First, SiC is a semiconductor and in presence of impurities like boron[40–42] or nitrogen[40,43,44] an increase of electrical conductivity due to doping of SiC is possible. As the composite ZS8, containing $ZrSi_2$ and ZrN but no boron compound (Table 2), revealed a similar resistivity to ZB8, doping of SiC by boron was excluded. In the case of nitrogen doping, electrical resistivities in the range of $10^{-2}\,\Omega$ cm were reported for a SPS-sintered SiC in presence of Si_3N_4.[43] Jeon[45] realized nitrogen doping in SiC (0.082 Ω cm at 800 °C) by a post heat treatment at 1700 °C in nitrogen atmosphere. These values were in good agreement with the resistivities of the $ZrSi_2$-containing composites in this work. Additionally, the $ZrSi_2$-containing composites showed a low temperature dependence of resistivity (Fig. 4), a resistivity behavior often described for nitrogen-doped SiC.[45–47] As the conducting network is a mixed one consisting of SiC grains and the ZrX_z phases, the resistivity will be decreased by an increased doping of the SiC grains. Contrary to the results, a lower local equilibrium nitrogen pressure inside the ZB composites compared to the ZN materials would be expected, possibly reducing the nitrogen doping. However, the higher Si activity might lead to additional defects of the carbon sites. Additionally, some co-doping of boron in addition to nitrogen might reduce the overall carrier concentration in the SiC grains resulting in lower conductivity. But based on the phase composition the same partial pressures and activities of B and N exist in the materials with the different ZrB_2 content. The observed reduction of the conductivity with decreasing ZrB_2 content could therefore also be connected with kinetics of the doping. However, all changes in the ZrX_z phase will have an impact on the composite resistivity because the different phases in ZB8 ($ZrSi_2$, Si, BN) compared to ZN8 (ZrN) could influence the doping of SiC.[45,48]

Secondly, it can be speculated on the formation of different resistivities at the grain boundaries SiC/SiC, SiC/$ZrSi_2$ and SiC/Si as well as SiC/ZrN. The Zr-Si phase was liquid during sintering probably affecting the structural and electrical properties of the ZrX_z/SiC contact areas that can strongly affect the overall resistivity.[38,39,49] Generally, low composite resistivities of about $10^{-1}\,\Omega$ cm were obtained for Si_3N_4–SiC based ternary composites including 8 vol.% of silicides[50] with melting points close to the sintering temperature like $ZrSi_2$, $MoSi_2$, WSi_2, $NbSi_2$ or $TaSi_2$. During sintering, the silicides are assumed to form liquid phases that strongly influence the SiC grain boundaries and lead to reduced contact resistivity. As the composite resistivity is a function of the grain and the grain boundary resistivities[39] ternary composites with a resistivity of about $10^{-1}\,\Omega$ cm have to have both, highly doped SiC grains and low grain boundary resistivities.

However, all discussed contributions on the composite resistivity cannot be completely separated.

4. Conclusion

The influence of 8 vol.% of ZrN or ZrB_2 on the Si_3N_4–SiC composite resistivity was investigated. During hot pressing ZrB_2 was not stable in the Si_3N_4–SiC matrix and decomposed to $ZrSi_2$, ZrN and BN whereas the addition of ZrN did not initiate any reactions. The composite containing ZrN offered a higher resistivity ($7 \times 10^3\,\Omega$ cm) compared to the composite that was modified by ZrB_2 ($3 \times 10^{-1}\,\Omega$ cm) addition. Due to a subsequent heat treatment, the composite resistivities decreased in the order of one magnitude for SC47, ZN8 and ZB8. By means of the composite ZB8–SN ($R > 10^7\,\Omega$ cm) it was shown that the lower resistivity of ZB8 did not originate from a ZrX_z percolation network. More likely, the conduction pathway was built up from SiC and ZrX_z grains, whereas differences in the resistivities might be referred to differences in the phase composition between ZB8 ($ZrSi_2$, Si, BN) and ZN8 (ZrN) having an influence on the doping of the SiC grains and on the grain boundary resistivities. The possibility to decrease the resistivity of Si_3N_4–SiC composites by adding low amounts of silicides is to be further investigated.

References

1. Klemm H. Silicon nitride for high-temperature applications. *SO: Journal of the American Ceramic Society* 2010;**93**:1501–22.
2. Jacobson NS. Corrosion of silicon-based ceramics in combustion environments. *Journal of the American Ceramic Society* 1993;**76**:3–28.
3. Klemm H, Taut C, Wotting G. Long-term stability of nonoxide ceramics in an oxidative environment at 1500 degrees C. *Journal of the European Ceramic Society* 2003;**23**:619–27.
4. Mclachlan DS, Blaszkiewicz M, Newnham RE. Electrical-resistivity of composites. *Journal of the American Ceramic Society* 1990;**73**:2187–203.
5. Mclachlan DS. Analytical functions for the dc and ac conductivity of conductor–insulator composites. *Journal of Electroceramics* 2000;**5**:93–110.
6. Kusy RP. Influence of particle-size ratio on continuity of aggregates. *Journal of Applied Physics* 1977;**48**:5301–5.
7. Malliari A, Turner DT. Influence of particle size on electrical resistivity of compacted mixtures of polymeric and metallic powders. *Journal of Applied Physics* 1971;**42**:614.
8. Kim WJ, Taya M, Yamada K, Kamiya N. Percolation study on electrical resistivity of SiC/Si_3N_4 composites with segregated distribution. *Journal of Applied Physics* 1998;**83**:2593–8.
9. Carmona F, Barreau F, Delhaes P, Canet R. An experimental-model for studying the effect of anisotropy on percolative conduction. *Journal de Physique Lettres* 1980;**41**:L531–4.

10. Carmona F, Canet R, Delhaes P. Piezoresistivity of heterogeneous solids. *Journal of Applied Physics* 1987;**61**:2550–7.
11. Tatami J, Katashima T, Komeya K, Meguro T, Wakihara T. Electrically conductive CNT-dispersed silicon nitride ceramics. *Journal of the American Ceramic Society* 2005;**88**:2889–93.
12. Yamada K, Kamiya N. High temperature mechanical properties of Si_3N_4–$MoSi_2$ and Si_3N_4–SiC composites with network structures of second phases. *Materials Science and Engineering A-Structural Materials Properties Microstructure and Processing* 1999;**261**:270–7.
13. Sawaguchi A, Toda K. Mechanical and electrical-properties of silicon-nitride silicon-carbide nanocomposite material. *Journal of the American Ceramic Society* 1991;**74**:1142–4.
14. Guo ZQ, Blugan G, Graule T, Reece M, Kuebler J. The effect of different sintering additives on the electrical and oxidation properties of Si_3N_4–$MoSi_2$ composites. *Journal of the European Ceramic Society* 2007;**27**:2153–61.
15. Kao MY. Properties of silicon-nitride molybdenum dislicide particulate ceramic composites. *Journal of the American Ceramic Society* 1993;**76**:2879–83.
16. Manukyan KV, Kharatyan SL, Blugan G, Kocher P, Kuebler J. $MoSi_2$–Si_3N_4 composites: Influence of starting materials and fabrication route on electrical and mechanical properties. *Journal of the European Ceramic Society* 2009;**29**:2053–60.
17. Sciti D, Guicciardi S, Bellosi A. Microstructure and properties of Si_3N_4–$MoSi_2$ composites. *Journal of Ceramic Processing Research* 2002;**3**:87–95.
18. Gao L, Li JG, Kusunose T, Niihara K. Preparation and properties of TiN–Si_3N_4 composites. *Journal of the European Ceramic Society* 2004;**24**:381–6.
19. Lee BT, Yoon YJ, Lee KH. Microstructural characterization of electroconductive Si_3N_4–TiN composites. *Materials Letters* 2001;**47**:71–6.
20. Liu CC, Huang JL. Micro-electrode discharge machining of TiN/Si_3N_4 composites. *British Ceramic Transactions* 2000;**99**:149–52.
21. Zivkovic L, Nikolic Z, Boskovic S, Miljkovic M. Microstructural characterization and computer simulation of conductivity in Si_3N_4–TiN composites. *Journal of Alloys and Compounds* 2004;**373**:231–6.
22. Jones AH, Dobedoe RS, Lewis MH. Mechanical properties and tribology of Si_3N_4–TiB_2 ceramic composites produced by hot pressing and hot isostatic pressing. *Journal of the European Ceramic Society* 2001;**21**:969–80.
23. Liu CC, Huang JL. Tribological characteristics of Si_3N_4-based composites in unlubricated sliding against steel ball. *Materials Science and Engineering A-Structural Materials Properties Microstructure and Processing* 2004;**384**:299–307.
24. Riedel R. Handbook of Ceramic Hard Materials. Weinheim: Wiley-VCH Verlag GmbH; 2000.
25. Hebsur MG. Development and characterization of SiC(f)/$MoSi_2$–Si_3N_4(p) hybrid composites. *Materials Science and Engineering A-Structural Materials Properties Microstructure and Processing* 1999;**261**:24–37.
26. Gräf I. Ionenätzen - Stand und Perspektiven für die Gefügekontrastierung keramischer und metallischer Werkstoffe - I. *Praktische Metallographie* 1998;**35**:235–54.
27. Gräf I. Ionenätzen - Stand und Perspektiven für die Gefügekontrastierung keramischer und metallischer Werkstoffe - II. *Praktische Metallographie* 1998;**35**:316–26.
28. Gräf I. Ionenätzen - Stand und Perspektiven für die Gefügekontrastierung keramischer und metallischer Werkstoffe - III. *Praktische Metallographie* 1998;**35**:359–83.
29. Hauffe W, Obenaus P, Herrmann M, Hapke J. Using the ion beam slope cutting technique for the examination of the microstructure of composite ceramics with extremely different components (BN/TiB_2) in the scanning electron microscope. *Praktische Metallographie* 2004;**41**:343–53.
30. Höhn S, Obenaus P, Hohlfeld J, Lies C. Phasencharakterisierung von Pulverpresslingen für Metallschäume mit dem Ionenstrahlpräparationsverfahren. *Prakt Metallogr Sonderband* 2007;**39**:161–6.
31. Petzow G, Herrmann M. Silicon nitride ceramics. Berlin: Springer-Verlag; 2002.
32. Talmy IG, Zaykoski JA, Opeka MM. High-temperature chemistry and oxidation of ZrB_2 ceramics containing SiC, Si_3N_4, Ta_5Si_3, and $TaSi_2$. *Journal of the American Ceramic Society* 2008;**91**:2250–7.
33. Park JH, Koh YH, Kim HE, Hwang CS. Densification and mechanical properties of titanium diboride with silicon nitride as a sintering aid. *Journal of the American Ceramic Society* 1999;**82**:3037–42.
34. Guo SQ. Densification of ZrB_2-based composites and their mechanical and physical properties: a review. *Journal of the European Ceramic Society* 2009;**29**:995–1011.
35. Monteverde F, Bellosi A. Effect of the addition of silicon nitride on sintering behaviour and microstructure of zirconium diboride. *Scripta Materialia* 2002;**46**:223–8.
36. Monteverde F, Guicciardi S, Bellosi A. Advances in microstructure and mechanical properties of zirconium diboride based ceramics. *Materials Science and Engineering A-Structural Materials Properties Microstructure and Processing* 2003;**346**:310–9.
37. Weng L, Zhang XH, Han JC, Han WB. The effect of Si_3N_4 on microstructure, mechanical properties and oxidation resistance of HfB_2-based composite. *Journal of Composite Materials* 2009;**43**:113–23.
38. Sauti G, Can A, McLachlan DS, Herrmann M. The AC conductivity of liquid-phase-sintered silicon carbide. *Journal of the American Ceramic Society* 2007;**90**:2446–53.
39. Siegelin F, Kleebe HJ, Sigl LS. Interface characteristics affecting electrical properties of Y-doped SiC. *Journal of Materials Research* 2003;**18**:2608–17.
40. Gubanov VA, Fong CY. Doping in cubic silicon-carbide. *Applied Physics Letters* 1999;**75**:88–90.
41. Pai CH. Thermoelectric properties of P-type silicon carbide. Xvii International Conference on Thermoelectrics. In: *Proceedings Ict, vol. 98*. 1998. p. 582–6.
42. Troffer T, Schadt M, Frank T, Itoh H, Pensl G, Heindl J, Strunk HP, Maier M. Doping of SiC by implantation of boron and aluminum. *Physica Status Solidi A-Applied Research* 1997;**162**:277–98.
43. Kado N, Kitagawa H, Ueda Y, Kanayama N, Noda Y. Preparation of p- and n-type SiC-based thermoelectric materials by spark plasma sintering. In: *Proceedings ICT'02. 21st International Conference on Thermoelectrics (Cat. No. 02TH8657)*. 2002. p. 163–5.
44. Liu HS, Fang XY, Song WL, Hou ZL, Lu R, Yuan J, Cao MS. Modification of band gap of beta-SiC by N-doping. *Chinese Physics Letters* 2009;**26**.
45. Jeon YS, Shin H, Lee YH, Kang SW. Reduced electrical resistivity of reaction-sintered SiC by nitrogen doping. *Journal of Materials Research* 2008;**23**:1020–5.
46. Shor JS, Goldstein D, Kurtz AD. Characterization of N-Type beta-SiC as a piezoresistor. *IEEE Transactions on Electron Devices* 1993;**40**: 1093–9.
47. Silva ACE, Kaufman MJ. Phase-relations in the Mo–Si–C system relevant to the processing of $MoSi_2$–SiC composites. *Metallurgical and Materials Transactions A-Physical Metallurgy and Materials Science* 1994;**25**: 5–15.
48. Kim KM, Seo SH, Kim JW, Song JS, Oh MH, Bahng W, Kim ED. The method for enhancing nitrogen doping in 6H–SiC single crystals grown by sublimation process: the effect of Si addition in SiC powder source. Stafa-Zurich: Trans Tech Publications Ltd.; 2006.
49. Ruschau GR, Yoshikawa S, Newnham RE. Resistivities of conductive composites. *Journal of Applied Physics* 1992;**72**:953–9.
50. Zschippang E. unpublished work, 2011.